Systematic Coarse Graining of 4-Cyano-4'-pentylbiphenyl

Grigorios Megariotis, Antonia Vyrkou, Adrien Leygue, Doros N. Theodorou

Systematic Coarse Graining of 4-Cyano-4′-pentylbiphenyl

Grigorios Megariotis, Antonia Vyrkou, Adrien Leygue, and Doros N. Theodorou*

Department of Materials Science and Engineering, School of Chemical Engineering, National Technical University of Athens, 9 Heroon Polytechniou, Zografou Campus, Athens 15780, Greece

A coarse-grained model is derived for a liquid-crystal-forming molecule, 4-cyano-4′-pentylbiphenyl (5CB), from a detailed atomistic model using the iterative Boltzmann inversion (IBI) method in the isotropic phase at 315 K and 1 bar. The coarse-grained model consists of five "superatoms" (one for the cyano group, two for the aromatic rings in the biphenyl moiety, and two for the alkyl tail), which are categorized as three types. A modification of IBI, wherein only one of the effective intermolecular potentials (the one corresponding to the superatom pair whose intermolecular correlation function exhibits the highest deviation from the atomistic one) is updated at each iteration, proves to be necessary to achieve convergence. The coarse-grained model, which enables a savings of a factor of 35 in computational cost relative to atomistic simulation, is used to explore ordering into liquid-crystalline phases at lower temperatures. It is found to yield a first-order ordering transition at 288 K with small hysteresis and negligible system size effects. A detailed investigation in terms of various structural and dynamical measurements indicates that the ordered phase is of the smectic type rather than nematic, as observed experimentally. The ordering temperature can be brought close to the experimental value of 308.5 K through the simple rescaling of the intermolecular effective interaction potentials employed in the coarse-grained model. A nematic ordered phase can be obtained from the coarse-grained model by scaling up the head−head and tail−tail effective interaction potentials obtained by IBI.

1. Introduction

Molecular simulations have been employed extensively over the last 2 decades to study soft matter (polymers, liquid crystals, colloids, surfactants, etc.). Despite the rapid increase of computing power available on modern machines and the possibility of massive parallelization, atomistic simulations are currently confined to a few hundreds of nanoseconds in molecular dynamics (MD) or a few hundred million moves in Monte Carlo simulations. To access the long time and length scales that govern the behavior of soft-matter systems, there is a need to change the level of description. This is the idea behind mesoscopic simulation methods, such as coarse-grained MD, Langevin dynamics, Brownian dynamics, lattice Boltzmann, dissipative particle dynamics, and dynamic density functional theory.[1−5] To retain a maximum level of predictive power, it is highly desirable that the models invoked in mesoscopic simulations be based directly on detailed atomistic ones. The derivation of a less detailed model, cast in terms of fewer degrees of freedom, from a detailed atomistic one is termed "coarse graining".

The idea of coarse graining has been widely used in molecular simulations.[6] In the present work, coarse graining entails the gathering of small units to form larger quasi-spherical entities, with the use of appropriate effective potentials among the newly defined larger entities (also called "beads" or "superatoms"). Even an atomistic model can be regarded as resulting from a coarse-graining procedure; the electrons are incorporated into their nuclei, and each atom is represented by a single sphere. Another familiar example of simple coarse graining is the commonly used united-atom or anisotropic united-atom representation,[7−9] in which hydrogens are absorbed by their vicinal carbons. An important advantage of such an approximation is the elimination of the fastest degrees of freedom, which are vibrational modes associated with the explicit hydrogens. In the same fashion, a mesoscopic model can be constructed from an atomistic one. Properties computed by mesoscopic models, such as elastic constants, viscosities, etc., can, in principle, be used as inputs to continuum models, which employ volume elements to represent a material.[10,11]

A variety of coarse-graining techniques have been presented in the literature. For polymer systems, iterative Boltzmann inversion (IBI) is a popular and rather straightforward method for constructing coarse-grained models.[12−19] Moreover, Müller-Plathe and co-workers have developed the automated simplex optimization method.[20−23] Biomolecules (proteins, lipids, DNA, etc.) constitute another area of significance in which phenomena cannot be captured by atomistic models because of the time and length scales on which they occur; hence, the development of accurate mesoscopic models is necessary.[24−27] An example of such a model, developed heuristically to match atomistic simulation results and experiment, is that of Marrink et al. for lipid-bilayer membranes.[24] A promising development in the field of systematic coarse graining is the force-matching method of Voth and collaborators, which has been applied successfully to lipid−water systems.[28−31] Coarse-grained models have also been developed systematically by the inverse Monte Carlo method.[32]

The objective of the work described in this article is systematically to coarse-grain a molecular system capable of forming thermotropic liquid-crystalline (LC) phases. This study is motivated by recent experiments that indicate that LC phases are capable of interrogating the structure of phospholipidic interfaces at the scale of nanometers,[33−35] thereby providing a powerful tool for probing the nanoscale structure and a basis for the development of sensors for biological molecules.[33] Because the time and length scales involved in these experiments are clearly out of the range of molecular simulations, there is a pressing need for reliable coarse-grained models. Liquid crystals, a class of substances with numerous and versatile applications in science and technology,[36,37] have been simulated extensively with coarse-grained models, based primarily on Gay−Berne ellipsoids.[38−43] Fewer simulations of thermotropic liquid crystals

* To whom correspondence should be addressed. E-mail doros@central.ntua.gr.

can be found in the literature based on detailed atomistic or united-atom models.[44−51] Attempts to develop coarse-grained models for LC systems by the application of a systematic method have been scarce.[52]

The particular LC system that we have chosen for our study is 4-cyano-4′-pentylbiphenyl (5CB), an archetypal example of small-molecule liquid crystals with numerous technological applications.[36,37] Extensive experimental studies are available for 5CB. A number of atomistic models have been developed for this system and for related systems in the bulk.[44−51] Our aim here is to develop a mesoscopic model for 5CB that will be optimized in the isotropic phase for some chosen structural and thermodynamic properties (radial distribution functions, intramolecular correlations, and density) and then test the ability of this model to capture the ordering transition and the structure and density of the ordered phase. The method we chose to apply for coarse graining is IBI. Specific questions we address are as follows: (a) Is it possible to coarse-grain 5CB in the isotropic phase, starting from a detailed atomistic model, through the IBI procedure? (b) If not, how can the IBI procedure be modified to achieve convergence to the target distribution functions? (c) Does a coarse-grained model so derived using structural information from the isotropic phase capture the first-order transition into the LC phase qualitatively and quantitatively? (d) How can the quantitative performance of the model in the ordered phase be improved? It has to be mentioned that this is the first time that the IBI method, as used for polymer systems, is applied in a LC system (5CB). A related method has been employed for nonbonded interactions in a previous study,[52] but in that case, the effective potentials were computed by simulating phases formed by fragments of the LC molecules.

This paper is organized as follows. The coarse-grained model that we developed is introduced in section 2. In section 3, we provide a brief description of the IBI method, discuss problems that we encountered with it, and introduce a modification that we designed in order to achieve convergence in the case of 5CB molecules. In section 4, we provide details on the simulations that we have conducted. The performance of our coarse-graining strategy in the isotropic phase is discussed in section 5, where convergence of the algorithm is quantified via appropriate figures and tables. Section 6 reports on our coarse-grained simulations of the ordering transition. Section 7 is devoted to a modification of our coarse-grained model aimed at improving the description of the ordered phase and to the structural and thermodynamic predictions that we obtained from the modified model. Section 8 summarizes the main conclusions from this study.

2. Molecular Models and Measurements of the Structures

All coarse-grained descriptions presented in this work have been developed from the same parent atomistic model, that of ref 51. The atomistic force field employs stretching, bending, and torsional intramolecular contributions along with Coulombic and Lennard-Jones intermolecular interactions. It adopts a united-atom representation for the alkyl tails and aromatic rings of the 5CB molecules. A total of 19 sites are used to represent each 5CB molecule.

In the coarse-grained (mesoscopic) model that we developed, the 19 atomistic sites were replaced by five superatoms. The coarse-grained representation is shown in Figure 1, along with an atomistic one. The first step toward the development of a coarse-grained model is *mapping*, i.e., defining the coordinates of each superatom on the atomistically represented molecule. At the mesoscopic level, the centers of superatoms CT1 and

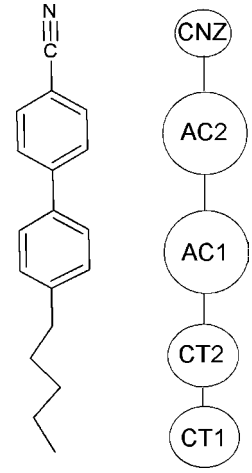

Figure 1. Detailed (19-site) and coarse-grained (five-bead) representations of a 5CB molecule. The lengths of the effective bonds CT1−CT2, CT2−AC1, AC1−AC2, and AC2−CNZ are 0.249, 0.380, 0.422, and 0.338 nm, respectively.

Table 1. Molar Masses of the Beads in a 5CB Molecule at the Mesoscopic Level

beads	molar mass (g/mol)	beads	molar mass (g/mol)
CT1	35.5	AC2	76.0
CT2	35.5	CNZ	26.0
AC1	76.0		

CT2 (group type CGCT) of the alkyl tail are placed at the positions of its second and fourth atomistic carbons, respectively. The positions of the superatoms AC1 and AC2 (group type CGAC), which represent the aromatic rings, are chosen to coincide with the atomistic centers of the rings, while the position of CNZ (group type CGCNZ) is chosen as the center of the atomistic C≡N bond. Table 1 provides the molar masses of the superatoms in the context of the mapping adopted here.

Now we turn our attention to the intramolecular potentials of a 5CB molecule at the mesoscopic level. Intramolecular potentials are applied here only for effective bending angles (θ) and distance (r)-dependent intermolecular interactions. Applying our coarse-graining strategy to a fully flexible mesoscopic model led to narrow Gaussian distributions of the effective bond lengths (l; see the Supporting Information). Using fixed effective bond lengths in place of these distributions left all structural and thermodynamic properties obtained at the mesoscopic level unchanged, while at the same time affording an increase in the time step for integration of the equations of motion of the mesoscopic model by more than a factor of 2. Thus, it was decided to use fixed l in the production phase of all coarse-grained simulations. The constant l values employed are given in the caption to Figure 1. As far as effective torsion angles (φ) are concerned, only torsion around the AC1−CT2 effective bond needs to be considered with the coarse-grained model adopted here. The difference between the minimum and maximum in the effective potential derived by Boltzmann inversion of this effective torsion angle, however, was much less than k_BT. Thus, no effective torsional potentials were incorporated in the coarse-grained model.

The number of intermolecular effective potentials required at the coarse-grained level is $n(n + 1)/2 = 6$, with $n = 3$ being the number of superatom types. The development of coarse-grained potentials could be based on nonbonded interactions, instead of intermolecular ones. In this study, however, we preferred to separate intermolecular nonbonded interactions from possible intramolecular nonbonded interactions. The six inter-

molecular potentials were developed by the iterative strategy described in sections 3 and 4 and stored as functions of separation r in tabular form.

We have evaluated an alternative coarse-grained model that, in addition to the superatoms and interactions described above, contained two partial charges on virtual atoms representing the carbon and nitrogen of the cyano group. The values of the partial charges reproduced the atomistic dipole moment of the 5CB molecule at the mesoscopic level. Good convergence to the target distribution functions was achieved for this coarse-grained model with explicit charges with the method described in sections 3 and 4. It was observed, however, that this model tended to form "glassy" phases, rather than ordered LC phases, upon cooling. This failure to predict the correct thermodynamic behavior can be explained on the basis of effective intermolecular potentials: The electrostatic interactions of the atomistic model have already been taken into account in deriving the effective potentials of the coarse-grained model (see also section 3); consequently, the use of explicit charges leads to double counting of the interactions in question. The model with explicit charges was therefore abandoned, and the simpler (and less expensive computationally) charge-free coarse-grained model outlined above was adopted for the production phase of our calculations.

Experimentally, 5CB is a uniaxial thermotropic LC molecule that displays only a nematic phase between its isotropic and crystalline phases. There are, however, other CB (cyanobiphenyl) molecules that exhibit both nematic and smectic phases (e.g., 8CB).[53,54] A central role in our analysis of ordering will be played by the Saupe ordering tensor,[55] defined by the following equation:

$$\mathbf{Q} = \frac{1}{N}\sum_{i=1}^{N}\left\{\frac{3}{2}\hat{\mathbf{u}}_i\hat{\mathbf{u}}_i - \frac{1}{2}\mathbf{1}\right\} \tag{1}$$

In eq 1, N is the number of molecules, $\hat{\mathbf{u}}_i$ is the unit vector along the axis of the ith molecule, and $\mathbf{1}$ is the unitary tensor of second order. The (dyadic) tensor $\mathbf{Q}$ is obtained as an instantaneous value for each configuration. The molecular axis is defined as the long axis obtained by diagonalization of the moment of inertia tensor,[56] $\mathbf{I}$:

$$\mathbf{I} = \sum_a m_a(r_a{}^2\mathbf{1} - \mathbf{r}_a\mathbf{r}_a) \tag{2}$$

Equation 2 is applied to each molecule, and the sum is taken over all atoms a that constitute one molecule. The atomic position vectors $\mathbf{r}_a$ are defined with respect to the molecular center of mass.

As defined, the tensor $\mathbf{Q}$ is symmetric and traceless, so it will have three real eigenvalues that sum to zero. In a phase characterized by cylindrical symmetry, $\mathbf{Q}$ will have one positive and two equal negative eigenvalues. As a criterion for the transition from the isotropic to the LC phase and vice versa, we will consider the order parameter S, defined as the largest eigenvalue of $\mathbf{Q}$. An alternative, but equivalent, definition of the order parameter equates it with -2 times the middle eigenvalue of the $\mathbf{Q}$ tensor.[57] In our ordered phases, the molecules will be oriented, on average, along a specific direction, which is specified by a unit vector called the director, $\mathbf{n}$. The director is defined here as that eigenvector of $\mathbf{Q}$ that corresponds to its largest eigenvalue. Instantaneous order parameters and directors are defined for each configuration and averaged over the production phase of a run.

Practically, values of the order parameter from 0.45 to 0.6 indicate the existence of a nematic phase.[58] In the isotropic phase, the order parameter tends to zero, with an increasing number of molecules N as $\sim N^{-1/2}$ (see section 5).

3. Coarse-Graining Method

The application of IBI presupposes a description of each molecule at the mesoscopic level as a set of superatoms. The many-body joint distribution function for all superatom coordinates could, in principle, be derived from atomistic simulation, and a potential of mean force could be defined by the logarithm of this joint distribution function. In place of the rigorous many-body potential of mean force, IBI uses a combination of effective potentials, each depending on a particular subset of the superatom degrees of freedom, to approximate it. The IBI procedure identifies this particular approximation as the unique decomposition that reproduces a particular set of lower-order distribution functions. In particular, it has been proven that there is a unique relationship between a pair potential and its corresponding radial distribution function (RDF).[32,59−61] In general, IBI considers contributions from effective bond lengths (l), effective bond angles (θ), and effective torsion angles (ϕ) formed by the superatoms, as well as distance-dependent effective intermolecular pair potentials between the superatoms. The results presented here were obtained with a model employing constant effective bond lengths and no effective torsional potentials. First estimates for the intramolecular bending potentials and for the intermolecular potentials between superatoms were obtained from the probability densities of the three θ's and the six intermolecular pair distribution functions between superatom types accumulated in the course of an equilibrated detailed atomistic simulation[12,13] (eqs 3 and 4):

$$U_1^{\text{bend}}(\theta) = -k_{\text{B}}T\ln[P(\theta)/\sin\theta] \tag{3}$$

$$U_{\alpha\beta,1}^{\text{inter}}(r) = -k_{\text{B}}T\ln[g_{\alpha\beta}(r)] \tag{4}$$

The functions $P(\theta)$ are atomistically computed intramolecular probability densities for the effective bond angles θ, while the factor $\sin\theta$ arises in the Jacobian of transformation from Cartesian to generalized coordinates.[62] Equation 4 contains a RDF, $g_{\alpha\beta}(r)$, for the pair of superatom species (α, β), obtained from the atomistic trajectory as well. In eqs 3 and 4, the prelogarithmic factor contains the temperature T of the system and the Boltzmann constant k_{B} (1.381×10^{-23} J/K), which emphasizes that $U_1^{\text{bend}}(\theta)$ and $U_{\alpha\beta,1}^{\text{inter}}(r)$ are not real potentials but configurational free energies. Additional temperature and density dependence arises from the distributions within the logarithmic factors.

Detailed descriptions of the IBI method are given in many previous simulation studies.[12−19] In our work, we found that the standard IBI method, when applied in the isotropic phase of 5CB in conjunction with the atomistic model discussed above, failed to converge (see Figure 2). This necessitated the development of a modified IBI method. Instead of globally updating all intermolecular effective potentials $U_{\alpha\beta}^{\text{inter}}$ at every iteration, our modified procedure updates only one $U_{\alpha\beta}^{\text{inter}}$ at a time. Specifically, each time we choose to modify that intermolecular effective potential that corresponds to the RDF of maximum error relative to the atomistically computed target RDF. A flow diagram of our modified IBI method is given in Scheme 1.

To correct the density or pressure of the system (depending on what ensemble is simulated), a ramp correction (or else "linear correction") was applied:

$$U_{\alpha\beta}^{\mathrm{corr}}(r) = U_{\alpha\beta}(r) - Ck_{\mathrm{B}}T\left(1 - \frac{r}{r_{\mathrm{c}}}\right) \quad (5)$$

The left-hand side of the previous equation contains the corrected intermolecular potentials $U_{\alpha\beta}^{\mathrm{corr}}(r)$ between the superatoms α and β. The second term on the right-hand side of eq 5 depends on the temperature and on the cutoff distance r_{c} of the intermolecular potentials, and C is an adjustable dimensionless parameter used to modify the pressure P. C is here taken to be the same for all pairs of superatom types. An estimate of C can be obtained through the pressure equation

$$PV = N_{\mathrm{mol}}k_{\mathrm{B}}T - \frac{1}{6V}\sum_{\alpha}\sum_{\beta}N_{\alpha}N_{\beta}\int_{0}^{+\infty} r\,\frac{\mathrm{d}U_{\alpha\beta}(r)}{\mathrm{d}r}\,g_{\alpha\beta}(r)\,4\pi r^{2}\,\mathrm{d}r \quad (6)$$

with N_{mol}, N_{α}, and V standing for the total number of molecules, the total number of superatoms of type α, and the volume of the system, respectively.

Substituting eq 5 in eq 6, the following equation in C is obtained:

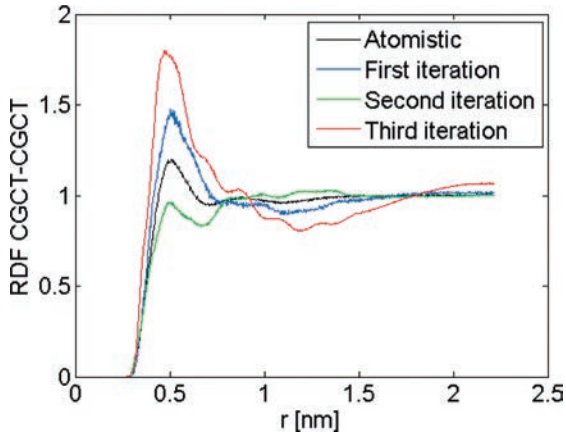

Figure 2. Divergence of the CGCT−CGCT RDF when all potentials are updated simultaneously at each IBI iteration.

Scheme 1. Flow Diagram for the Modified IBI Method

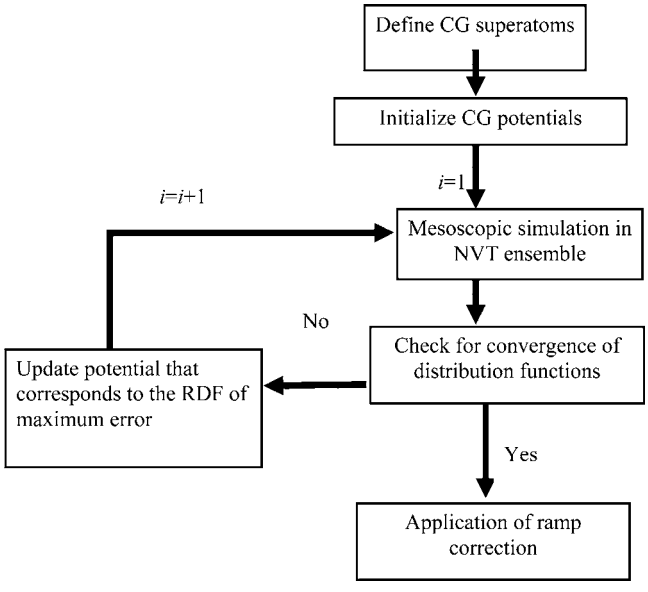

$$V\Delta P = -\frac{2\pi}{3}\frac{Ck_{\mathrm{B}}T}{Vr_{\mathrm{c}}}\sum_{\alpha}\sum_{\beta}N_{\alpha}N_{\beta}\int_{0}^{r_{\mathrm{c}}} g_{\alpha\beta}(r)\,r^{3}\,\mathrm{d}r \quad (7)$$

ΔP represents the difference between the target (atomistic) value of pressure and the value derived from a coarse-grained simulation using IBI effective potentials. The need to adjust the pressure after implementation of IBI is attributed to the fact that the virial pressure is not retained upon coarse graining, even if the atomistically derived $g_{\alpha\beta}(r)$ functions are reproduced.[29] In eqs 5 and 7, r_{c} and the adjustable dimensionless parameter C are defined to be the same for all superatom pairs (α, β).

4. Simulation Details

All simulations were performed with the MD package[63−65] *GROMACS 3.3.2*. Effective bond lengths in the coarse-grained model were constrained to their average values using the *SHAKE*[66] algorithm (relative tolerance 10^{-5}). This allowed the use of a time step of 20 fs. By comparison, the time step used in connection with the atomistic model was 2 fs.[51] The atomistic trajectories employed in this work were produced by repeating all simulations in the *GROMACS* package with the same simulation details as those reported in ref 51 except for the time step, which was equal to 2 fs in our simulations. All structural and thermodynamic information derived from our atomistic simulations was within error bars of those reported in ref 51.

The coarse-grained MD simulations involved in the IBI iterations were conducted in the *NVT* and *NPT* ensembles using the Nosé-Hoover thermostat[67,68] with a time constant equal to 1.0 ps. In the *NPT* ensemble, the simulation box was kept rectangular and the pressure was set to $P = 1$ bar using the *GROMACS*[65] version of the Parrinello−Rahman barostat[69,70] with a time constant equal to 4.0 ps. In order to obtain accurate structural properties, free of statistical noise, every IBI iteration involved a coarse-grained MD simulation of one million steps.

For the intermolecular interactions of the coarse-grained model, a simple cutoff scheme was employed with a r_{c} distance equal to 1.5 nm, where intermolecular potentials tend to zero or, equivalently, the RDFs between superatoms tend to unity. These interactions, as obtained by the IBI method, were stored in tabular form, and a smoothing via Chebyshev polynomials[71,72]

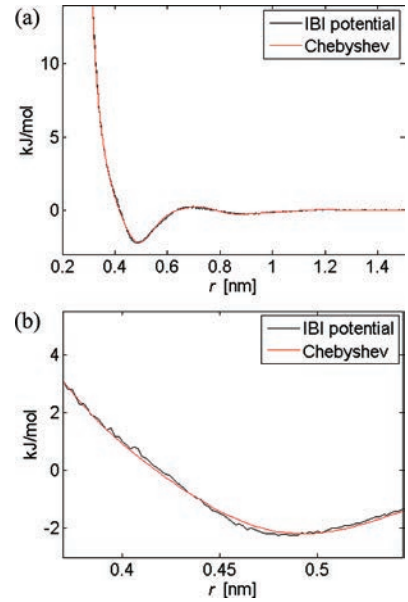

Figure 3. (a) Example of a fitting (for the CGAC−CGCNZ potential) by Chebyshev polynomials. (b) More detailed snapshot of the fitting.

Table 2. Relative Errors (%) (eq 8) of the RDFs for Three Different Iterations

	CGCT−CGCT	CGCT−CGAC	CGCT−CGCNZ	CGAC−CGAC	CGAC−CGCNZ	CGCNZ−CGCNZ
RE_1[a]	2.56	0.71	1.93	1.00	0.294	2.08
RE_2[b]	1.08	0.340	0.861	1.40	1.76	0.751
RE_{15}[c]	0.111	0.0862	0.0584	0.153	0.100	0.104

[a] Relative error of the first iteration in the *NVT* ensemble. [b] Relative error of the second iteration in the *NVT* ensemble. [c] Relative error of the 15th iteration in *NPT* ensemble.

was applied (full details are given in the Supporting Information). The effectiveness of this method is depicted in Figure 3, where a noisy effective potential is approximated by a smooth function. Intramolecular interactions were fitted by functional forms available in *GROMACS 3.3.2* (see also the Supporting Information for effective bending potentials). In all cases, the fitting involved a least-squares approximation of the numerical potentials.

The excluded volume region, readily detected in the RDFs between superatoms, was described by a simple repulsive potential of an inverse 12th degree (A/r^{12}). The parameter A was computed under the demand of continuity between this extrapolated repulsive potential and the IBI potentials at the connection point. The best value of parameter C in the ramp correction of eq 5 was found to be equal to 1.5×10^{-4}.

Because of the elimination of some degrees of freedom for 5CB, the dynamics appears faster in comparison to that of the atomistic model. In order to obtain similar self-diffusivities of 5CB between the two levels of description, a friction force is introduced in the context of Langevin dynamics. The friction constant value that proved to work well in this work equals 4.5 ps^{-1}. Details on how stochastic dynamics is applied are given in ref 65. All other parameters are exactly the same as those of the MD simulations, reported above.

The IBI method was initially applied to a coarse-grained system of 216 5CB molecules in the isotropic phase (315 K and 1 bar). In addition, in order to check for possible system size effects on structural properties, larger isotropic systems of 5CB, consisting of 432, 864, and 1728 molecules, were simulated at the coarse-grained level. Initial configurations for these systems were constructed by appropriate transformations of the primary simulation box of 216 molecules. Neither distribution functions nor density exhibited any dependence on the size of the simulated system.

After the development of the coarse-grained model in the isotropic phase, the structure of the system was investigated in the LC region. To this end, MD simulations were conducted with the temperature changing linearly with time at a prescribed rate of cooling or heating (annealing mode of *GROMACS*).[65] All other conditions of the ordering coarse-grained simulations were exactly the same as those reported above for simulations of the isotropic phase.

5. Performance of the Coarse-Graining Algorithm in the Isotropic Phase

In this section, we first discuss the ability of the developed coarse-grained model to reproduce the chosen atomistic structural properties in the isotropic phase of 5CB at 315 K and 1 bar. The crucial part for developing this model was the convergence of RDFs. For this reason, the iterative coarse-graining procedure was monitored via relative errors defined by the following equation:

$$\mathrm{RE} = \frac{\int_0^{r_c} w_{\alpha\beta}(r)\,[g_{\alpha\beta,i}(r) - g_{\alpha\beta}(r)]^2\,\mathrm{d}r}{\int_0^{r_c} w_{\alpha\beta}(r)\,[g_{\alpha\beta}(r)]^2\,\mathrm{d}r} \qquad (8)$$

The RDFs of the ith iteration and the atomistic target function for superatom pair (α, β) are symbolized by $g_{\alpha\beta,i}(r)$ and $g_{\alpha\beta}(r)$, respectively. The weighting function $w_{\alpha\beta}(r)$ in these integrals may be used to give more weight to some points of the grid. In our case, this function was set equal to $\exp(-r/r^*)$ with $r^* = 1$ nm. Table 2 lists the relative errors for all RDFs for the first, second, and final iterations of the IBI method. It is concluded from the third row of the aforementioned table that a high quality of convergence was achieved. The success of the modified IBI method is also shown clearly in Figure 4, where three of the six RDFs are presented (see the Supporting Information for the other three). In each diagram, three lines are depicted, displaying the $g_{\alpha\beta}(r)$ obtained from the atomistic simulation, the $g_{\alpha\beta,1}(r)$ from the first iteration of the IBI algorithm, and the final converged distribution function $g_{\alpha\beta,15}(r)$ describing the structure at the mesoscopic level. A reminder of how the IBI algorithm is started would perhaps be useful here. First, the RDFs and intramolecular distributions are computed by the atomistic model for the given mapping. Second, the aforementioned quantities are substituted in eqs 3 and 4. With this procedure, the first set of intra- and intermolecular potentials are available so as to start the first simulation (i.e., first iteration of IBI) at the mesoscopic level.

As far as the density of the system at the mesoscopic level is concerned, there is very good agreement with both the parent atomistic model[51] and experimental measurements.[73] Although the optimization procedure took place at a specific temperature (315 K), we present in Figure 5 the results for three different temperatures in the isotropic phase. In addition, the densities are compared with those reported for another atomistic model.[49]

It is instructive to examine system size effects on the order parameter S of the isotropic phase. To this end, we have simulated systems of 216, 432, 864, and 1728 5CB molecules at the coarse-grained level at 315 K and 1 bar. S was obtained by diagonalizing the instantaneous $\mathbf{Q}$ tensor in each recorded configuration and then averaging over all configurations in the equilibrated portion of a run. The statistical error on S thus obtained was also estimated by block averaging[74] over the equilibrated portion of the run. The results are presented in Figure 6. They can be fitted to an excellent approximation with an expression of the form $S(N) = \text{constant}/N^{1/2}$. In the isotropic phase, S, which is nonnegative by definition (compare the discussion in section 1), behaves as a fluctuation quantity converging to its thermodynamic limit of 0 as $N^{-1/2}$.

Closing this section, it has to be mentioned that the diffusion constant of 5CB is not retained upon coarse graining. In particular, it is greater in the case of the coarse-grained model (2.9×10^{-5} cm^2/s) in comparison with the corresponding atomistic value (5.5×10^{-6} cm^2/s). This problem can be alleviated by applying stochastic dynamics instead of MD. Now, a friction and a random force are introduced so that the dissipation−fluctuation theorem is satisfied.[75] The value of the friction constant used in our coarse-grained stochastic dynamics simulations was reported in section 4; for this value, the diffusion constant equals 5.3×10^{-6} cm^2/s. At this point, it has to be stressed that the correction of the self-diffusion constant was based on a trial-and-error procedure rather than on a

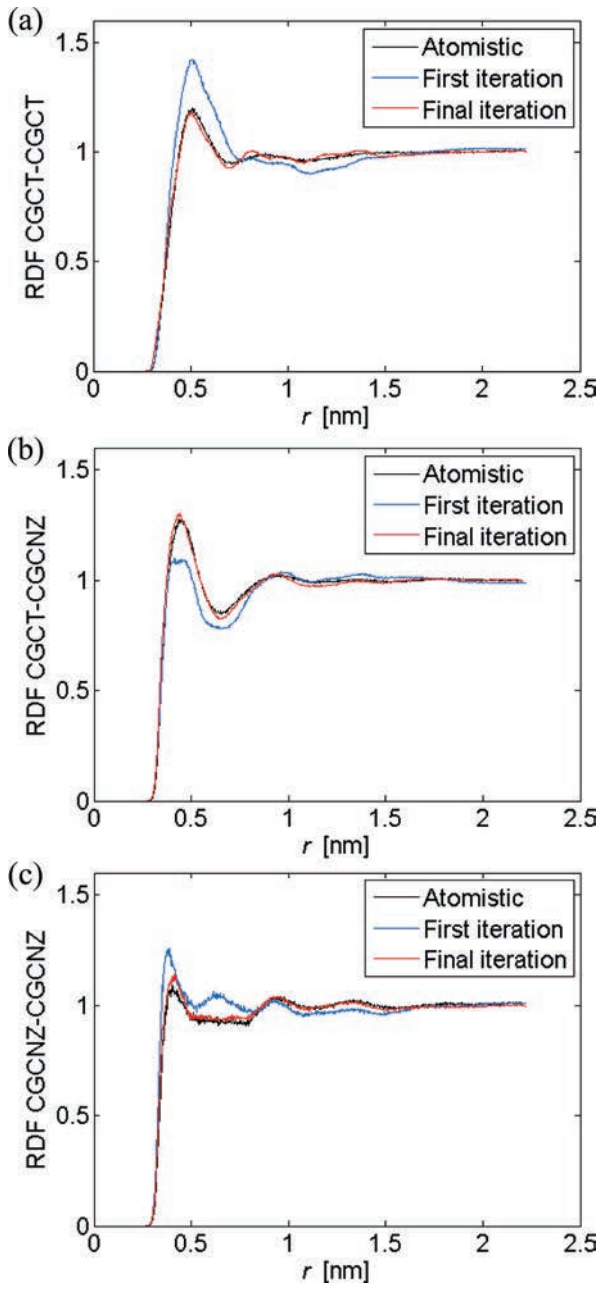

Figure 4. RDFs of the pairs (a) CGCT−CGCT, (b) CGCT−CGCNZ, and (c) CGCNZ−CGCNZ for the first and final iterations of the modified IBI method and a comparison with the target atomistic RDF.

systematic technique for dynamical coarse graining, such as the projection operator formalism.[1,2,76,77] An interesting discussion of how this more rigorous formalism can be applied in computer simulations can be found in ref 78.

6. Coarse-Grained Simulations of the Ordering Transition

We now turn our attention to the ability of the coarse-grained model, as developed by our modified IBI method in the isotropic phase, to predict characteristics of the ordering transition and of the LC phase of 5CB.

Isobaric cooling MD simulations of our IBI-based model, started in the isotropic phase, led readily to ordering, detectable by discontinuous increases in the order parameter S (large) and the density (small). A schematic representation of the isotropic and LC phases at the mesoscopic level is provided in Figure 7.

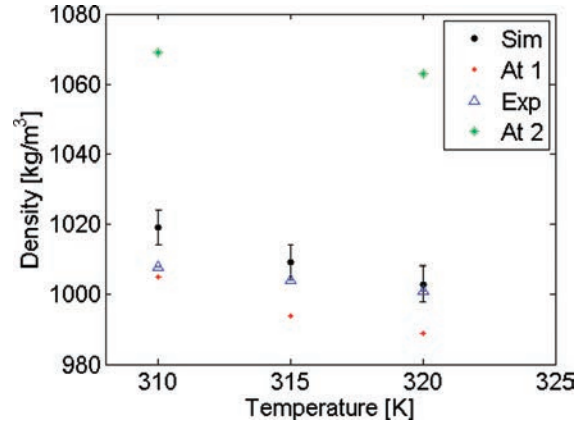

Figure 5. Comparison of orthobaric densities in the isotropic phase, as obtained from *NPT* simulations using the IBI-based model (Sim), with other (atomistic) simulation results (At1, parent atomistic model;[51] At2, atomistic model of ref 49) and with experiment[81] (Exp).

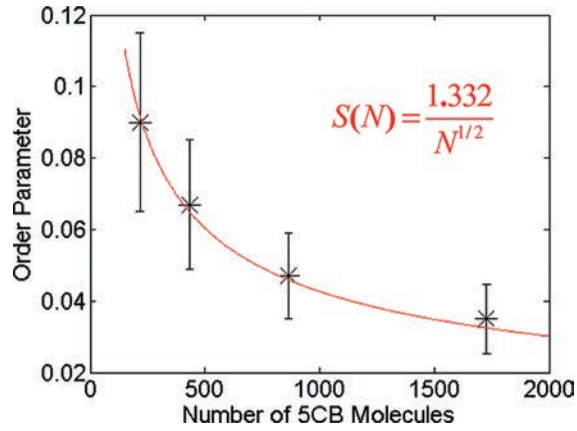

Figure 6. Order parameter S as a function of the number N of 5CB molecules in the model system and a least-squares approximation of the same order parameter for the IBI-based model in the isotropic phase at 315 K and 1 bar.

In this figure, each 5CB molecule is represented by a vector connecting the superatoms AC1 and CNZ. The ordering is visually obvious.

To estimate the first-order transition points from the isotropic to LC phase and vice versa, we conducted coarse-grained MD at decreasing and increasing temperatures. Initially, an isobaric MD simulation was undertaken with a cooling rate of 0.3 K/ns starting from the isotropic phase at 300 K and 1 bar and ending at 278 K. An isobaric heating simulation back to 300 K followed at the same heating rate, 0.3 K/ns. Results from the latter cooling/heating computer experiment are shown in Figure 8. It can be concluded from this figure that the transition points of the IBI-based coarse-grained model from the isotropic to LC phase and vice versa are 281 and 295 K, respectively. As the number of 5CB molecules in the model system increases, the cooling and heating rates for the temperature annealing must be lowered to maintain the width of the hysteretic region. Such a hysteresis in the ordering phase transition is not seen experimentally; nevertheless, it is not too large, given the high rates of cooling and heating (compared to the laboratory rates) employed in the simulations. We can estimate the equilibrium temperature for the coexistence of disordered and LC phases of our coarse-grained model as an average from the estimates obtained from cooling and heating simulations, i.e., 288 K. The hysteresis region can be made narrower by reducing the cooling/heating rate. To explore this, we undertook constant temperature

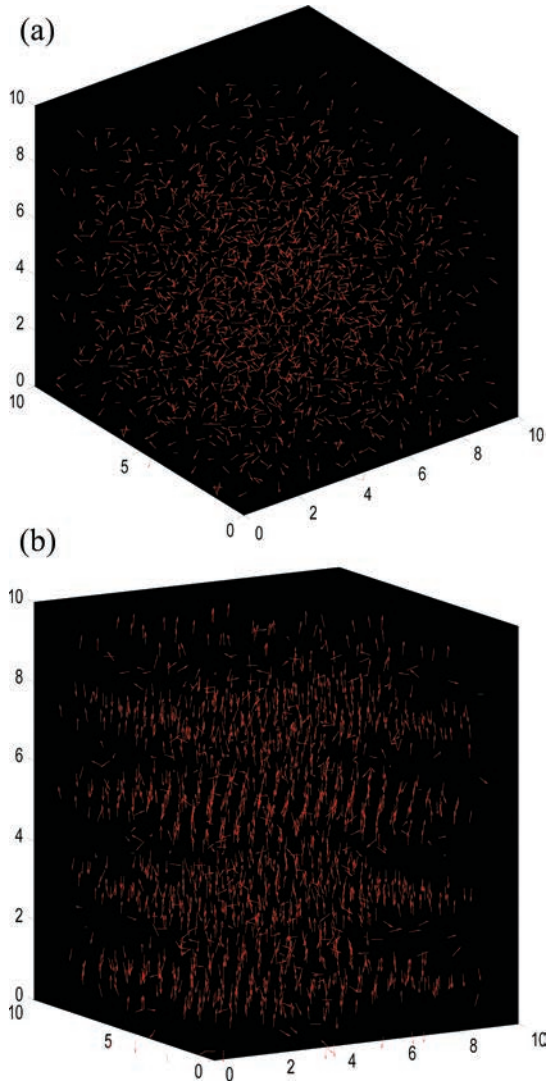

Figure 7. Total of 1728 5CB molecules, represented by vectors connecting beads AC1 and CNZ: (a) in the isotropic phase at 315 K and 1 bar; (b) in the LC phase at 275 K and 1 bar (IBI-based model, box dimensions in nanometers).

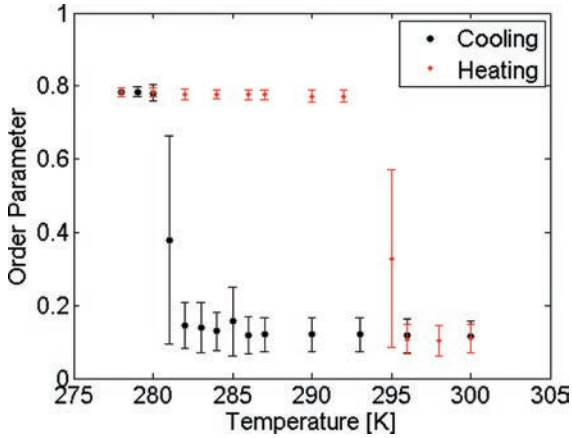

Figure 8. Evolution of the order parameter with the temperature during cooling and heating runs at 1 bar on the IBI-based model from 300 to 278 K and vice versa. The cooling and heating rates were 0.3 K/ns.

simulations in this region. An initial isotropic phase was found to change into a smectic phase after 720 ns of constant-temperature MD at 285 K, while a smectic phase was found to disorder into an isotropic one after 40 ns of constant-temperature simulation at 292 K. The atomistic model that served as a basis for our coarse-grained model[51] yields a nematic-to-isotropic transition temperature very close to the experimental value of 308.5 K. We conclude that our coarse-grained model with parameters developed to match the atomistic structure in the isotropic phase at 315 K underestimates the transition temperature by 20 K. This observation underlines the difficulty of capturing the ordering transition correctly with IBI-based models. Another interesting observation is that the transition is indeed of first order from a thermodynamics point of view. The reader may have noticed our use of the term "liquid-crystalline phase", rather than "nematic phase", for the phase obtained by cooling. This is intentional because the structure of this ordered phase will have to be investigated. Moreover, some important properties of the LC phase are compared and discussed with those obtained from a modified approach in the next section. At this point, one can speculate about the inability of the original model to predict the nematic phase. CB liquid crystals can produce different LC phases according to the length of their alkyl tail. For instance, 5CB forms a nematic phase, while 8CB can be ordered both in nematic and smectic phases. In our case, because of the use of a simple and coarse-grained model for 5CB, the flexibility of the alkyl tail is not reproduced perfectly, and consequently the nematic phase is not formed.

7. Improved Coarse-Grained Models and the LC Structure Obtained from Them

7a. Approach to the Smectic Phase. From the above analysis, an important question arises: Can our IBI-based model be modified so as to give a transition temperature close to the experimental value for 5CB? Such a modification (modified model I) was attempted by rescaling the intermolecular interaction potentials (eq 9). In particular, only the intermolecular potentials were changed according to the following scheme:

$$U_{\text{modified}}(r) = aU(r) \tag{9}$$

The prefactor a, common to all coarse-grained intermolecular potentials, was estimated through a trial-and-error procedure, until the predicted transition temperature was within 6 K of the experimental value $T_{\text{NI}}^{\text{EXP}}$(308.4 K). Again, all intermolecular potentials $U_{\text{modified}}(r)$ were determined in tabular form. In particular, a MD simulation with increasing temperature was undertaken (heating rate equal to 0.3 K/ns), starting from 275 K. The pressure was kept at 1 bar in all three directions. When the prefactor α is equal to 1.05, a very satisfactory transition point (302 K) is obtained. In addition, with the above set of modified potentials, a new ramp correction was applied ($C = -1.0 \times 10^{-5}$) so as to adjust the density.

Having defined the parameter a, we have a set of intermolecular potentials available in tabular form that allow a study of the modified model in the LC region at higher temperatures than those where a LC phase is observed with the IBI-based model. All simulation results for the LC phase, in the context of the modified model, were collected at 300 K, where the system of coarse-grained 5CB molecules is found in the ordered phase. As regards the orientation of the director, this stays practically unchanged during simulations, as indicated by the normalized autocorrelation function $C(t) = \langle \mathbf{n}(0) \cdot \mathbf{n}(t) \rangle$ [$C(t) >$ 0.994 for the longest simulation time accessed], depicted in Figure 9. In addition, the same quantity is presented for the IBI-based model at 275 K for a modified model, designed to give a nematic phase at 300 K (for more details, see the next subsection).

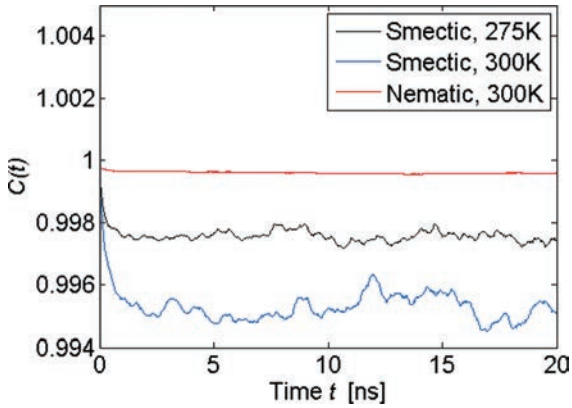

Figure 9. Comparison of the normalized time autocorrelation function of the director in the smectic phases (IBI-based model at 275 K and modified model at 300 K) and in the nematic phase at 300 K.

Table 3. Diffusion Constants along the Director and in a Plane Normal to the Director for the Coarse-Grained Models under Study[a]

T (K)	$D_{\|}/D_{\perp}$
275	0.049 ± 0.027
300	0.22 ± 0.06
300	1.149 ± 0.450

[a] The first row refers to the IBI-based model at 275 K and the second and third rows to the modified models in smectic and nematic phases, respectively, at 300 K.

A detailed analysis of some important properties was undertaken to characterize the structure of the LC phase. These properties were computed for both the original IBI-based (section 6) and modified coarse-grained model I (present section) at two different temperatures (the modified model at 300 K and the IBI-based model at 275 K). We started with the self-diffusion behavior of LC molecules in the coarse-grained system. In view of the strong anisotropy, separate self-diffusion coefficients were computed along the director and in the plane perpendicular to the director. An important quantity, presented in Table 3, is the ratio of these two diffusion coefficients, $D_{\|}/D_{\perp}$. It is seen that $D_{\|} < D_{\perp}$ for both coarse-grained models, which is evidence for the existence of a smectic phase.[79] In nematic phases, the following inequality holds: $D_{\|} > D_{\perp}$. Thus, the self-diffusion behavior, along with the layered structure observed visually in our ordered phases (see Figure 7b), gives us a first indication for a smectic phase. Some quantitative measurements of the structure are needed as well, however.

The first structural property presented is the probability density of the angle θ between the molecular axis and the director, divided by the factor $\sin(\theta)/2$ (see Figure 10). The latter factor is the probability density expected of an isotropic phase, where molecular orientations are random. Three main conclusions are derived from Figure 10: First, there is a strong tendency for molecules to orient parallel or antiparallel to the director. Second, parallel and antiparallel orientations are equally probable. Third, the existence of a smectic C phase is excluded; in such a smectic phase, the director does not coincide with the normal to the layers. The reduced distribution of orientation angles is plotted in Figure 10 at two different temperatures (275 and 300 K for the IBI-based model and its modification, respectively), but corresponding diagrams at different temperatures in the smectic phase are very similar.

Another important structural property is the distribution of molecular centers along the director, depicted in Figure 11. From the form of this distribution, it is clear that we have a layered

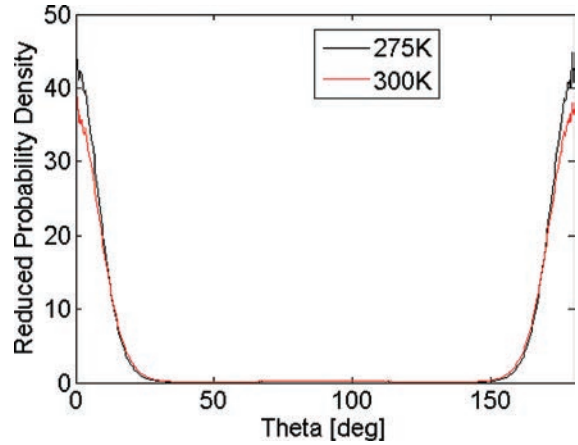

Figure 10. Comparison of probability densities of angle θ between the molecular axis and director divided by the factor $(\sin \theta)/2$ for the two coarse-grained models (the IBI-based model at 275 K and the modified model I at 300 K).

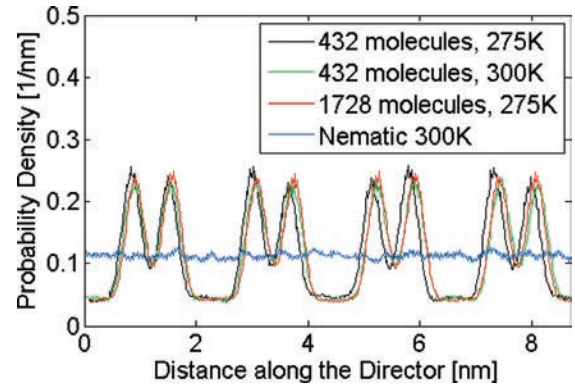

Figure 11. Comparison of the distributions of 5CB molecular centers along the director for three models (the IBI-based model at 275 K and modified models I and II at 300 K). At 275 K, possible size effects were checked.

structure. This further supports the evidence presented above for a smectic phase. In the same figure, we have plotted the distributions that we obtained by simulating systems of 432 and 1728 molecules with the IBI-based model. The distributions are very similar, confirming the absence of system size effects. The difference between these distributions and the distribution obtained for the IBI-based model at 275 K is insignificant. One can discern two characteristic distances in the distributions of Figure 11. This tells us that the smectic phase formed by the coarse-grained model actually consists of bilayers made up of antiparallel 5CB molecules. Such a structure consisting of bilayers of antiparallel molecules is observed in the smectic phase of 8CB.[80] Unfortunately, the smectic structure predicted by the coarse-grained model at 1 atm and 300 K is not in agreement with experiments and simulations with the parent atomistic model[51] of 5CB, which give a nematic phase under these conditions.

To confirm that the smectic phase is actually the equilibrium phase of our coarse-grained model at low temperature, we generated a nematic configuration of 216 5CB molecules at 300 K and 1 bar by atomistic simulation; replicated it periodically to generate a quadruple system; replaced the atomistically represented molecules in the resulting system by coarse-grained molecules; and proceeded to simulate the coarse-grained system with isothermal−isobaric MD under the same conditions. The coarse-grained model system readily converted from the nematic to a smectic phase, characterized by the structural features discussed above.

Table 4. Densities and Order Parameters in the Nematic Phase

	modified model II	atomistic model[51]	exptl[54,82]
density [kg/m^3]	1035 ± 3	1028	1020
order parameter	0.512 ± 0.004	0.54	0.54

7b. Approach to the Nematic Phase. In the previous subsection, we provided a methodology that allows us to correct the transition temperature with good consistency between the original and modified approaches. However, the ordered structure predicted for 5CB by our coarse-grained model under ambient conditions is incorrect, as pointed out in the previous section. For this reason, we designed a heuristic approach, based on a rescaling of the potentials as described by eq 9, to develop an alternative coarse-grained model that will give a nematic phase at 300 K and 1 atm. Our choice is to rescale only the potentials CGCT−CGCT (tail−tail) and CGCNZ−CGCNZ (head−head) with the parameter α equal to 1.2. For the remaining potentials, a ramp correction ($C = -8 \times 10^{-6}$) was applied to adjust the density of the system.

Order parameter and density are two crucial parameters that can be compared directly against the parent atomistic model. The comparison in question is recorded in Table 4. Moreover, some additional properties were checked in order to judge the quality of the nematic phase. First, the stability of this phase is explicitly depicted in Figure 9, in which the normalized autocorrelation function of the director is recorded. The smooth appearance of this function in relation to those shown in the same figure for the smectic phase is ascribed to the fact that results from a much larger system (1728 molecules) are depicted in the case of the nematic phase. All ordered phases examined in Figure 9 are clearly very stable because the aforementioned autocorrelation functions of the director remain close to unity. Another criterion that we have a nematic phase is the ratio of the diffusion constants along the director and normal to the director. In Table 3, it is seen that this quantity $D_{\|}/D_{\perp}$ is greater than unity for the nematic phase that we constructed. Futhermore, the phase does not have a layered structure, as is seen in Figure 11.

8. Conclusions

A coarse-grained model of 5CB molecules has been developed in this study based on simulations of a detailed atomistic model[51] at 1 bar and 315 K, where 5CB is found in the isotropic phase. The IBI method had to be modified to achieve convergence in our case (liquid of small, strongly polar molecules consisting of three types of coarse-grained sites). Important elements of the modified IBI strategy were (a) a conservative updating scheme, which updates only one (the poorest) effective intermolecular potential at a time, instead of the common global update and (b) the use of Chebyshev polynomials and of a r^{-12} excluded volume repulsion at short distances to fit the pretabulated numerical effective intermolecular interaction potentials and eliminate the adverse effects of noise in these potentials. The algorithm that we have designed, built around the MD engine of *GROMACS 3.3.2*, is rather fast, requiring 15 iterations to reproduce the structure and density to within 0.2% and 1.5% of the atomistic simulation, respectively.

In general, the main aim of a coarse-grained model is to augment the time and length scales that can be addressed by simulation. The coarse-grained model that we have developed can be used with a time step of 20 fs, instead of 2 fs required at the atomistic level. Moreover, the degrees of freedom for a 5CB molecule have been reduced drastically to the coordinates of 5 superatoms subject to 4 holonomic effective bond length constraints, in place of 19 atoms in the original united-atom representation. Using this coarse-grained model, our simulations were readily extended up to a simulation box 8 times bigger than the atomistic box of 216 molecules for times of 1 μs. Overall, the coarse-grained model is roughly 35 times more efficient computationally on a single processor than the atomistic model from which it was derived. Of course, simulations of even bigger systems can easily be achieved via parallelization. In addition, we point out that the mesoscopic models presented here do not require electrostatic interactions. Consequently, given the nonideal scaling characterizing commonly used algorithms for electrostatics, they offer an additional advantage for parallelization in comparison with the atomistic model.

We have performed MD simulations of our coarse-grained model, developed in the isotropic phase at 315 K and 1 bar, in order to investigate its ability to predict a transition to a LC phase and the structure of that phase. Our IBI-based model was found to underestimate the transition temperature from the isotropic to oriented phase and vice versa by roughly 20 K. To remedy this, two modified models were developed by heuristic rescaling of the effective intermolecular interaction potentials of the IBI-based model. The first modified model still gives a smectic phase but predicts a transition point of 302 K with relatively small hysteresis (6 K), in good agreement with experiment (308.5 K). On the basis of the order parameter, the predicted transition of this model is clearly first order from a thermodynamic point of view. A number of structural and dynamical characteristics of the LC phase were computed, including the distribution of angles formed with the director, the distribution of molecular centers of mass along the director, and self-diffusivities along and normal to the director. All of these measurements indicate that the ordered structure in the LC phase is smectic. Real 5CB, however, as well as the parent atomistic model, undergoes a transition from the isotropic to nematic phase. For this reason, through a heuristic modification of two effective pair potentials, we developed another modified model II, which predicts a nematic phase around 300 K. The order parameter and density for this model are very close to the atomistic model and the experimental predictions.

Longer CB molecules (e.g., 8CB) form both nematic and smectic phases in their LC region. In view of this, our modified models may be appropriately extended to simulate such liquid crystals. In addition, we intend to simulate the interface water−5CB in the mesoscopic model (300 K) by using modified model II, which gives the correct phase from a thermodynamic point of view, in conjunction with a coarse-grained water model already available in the literature. Our work so far indicates that Marrink's coarse-grained water model is satisfactory in this respect.[24] After coupling the two coarse-grained models, we apply an optimization technique that minimizes deviations from the structural features of the interface computed by the atomistic model, to determine coarse-grained parameters for the water−5CB interactions. Also, a systematic procedure of deriving a nematic phase (without modifications in the intermolecular potentials) is being investigated.

Acknowledgment

Financial support from the European Commission via the EU-NSF Specific Targeted Research Project "Modelling Nanostructured Interfaces for Biological Sensors" (MNIBS; Project NMP3-CT-2005-016375) is gratefully acknowledged.

Supporting Information Available: Details of the coarse-graining procedure and additional results from our coarse-

grained simulations of the isotropic and LC phases of 5CB: (S.1) divergence of the standard IBI scheme in the case of 5CB; (S.2) effective intermolecular potentials, as obtained from the modified IBI procedure in the isotropic phase of 5CB; (S.3) convergence of intramolecular distribution functions upon application of the modified IBI scheme to the isotropic phase of 5CB. This material is available free of charge via the Internet at http://pubs.acs.org.

Literature Cited

(1) Zwanzig, R. J. Ensemble Method in the Theory of Irreversibility. *Chem. Phys.* **1960**, *33*, 1338.

(2) Mori, H. Transport, Collective Motion and Brownian Motion. *Prog. Theor. Phys.* **1965**, *33*, 423.

(3) Carmesin, I.; Kremer, K. The Bond Fluctuation Method: a New Effective Algorithm for the Dynamics of Polymers in all Spatial Dimensions. *Macromolecules* **1988**, *21*, 2819.

(4) Groot, R. D.; Warren, P. B. Dissipative Particle Dynamics: Bridging the Gap between Atomistic and Mesoscopic Simulation. *J. Chem. Phys.* **1997**, *107*, 4423.

(5) Fraaije, J. G. E. M.; van Vlimmeren, B. A. C.; Maurits, N. M.; Postma, M.; Evers, O.; Hoffmann, C.; Altevogt, P.; Zvelindovsky, A. V.; Goldbeck-Wood, G. The Dynamic Mean-Field Density Functional Method and its Application to the Mesoscopic Dynamics of Quenched Block Copolymer Melts. *J. Chem. Phys.* **1997**, *106*, 4260.

(6) Nielsen, S.; Lopez, C.; Goundla, S.; Klein, M. J. Coarse Grain Models and the Computer Simulation of Soft Materials. *J. Phys.: Condens. Matter* **2004**, *16*, R481.

(7) Martin, M. G.; Siepmann, J. I. Transferable Potentials for Phase Equilibria United-Atom Description of *n*-Alkanes. *J. Phys. Chem. B* **1998**, *102*, 2569.

(8) Nath, S. K.; Escobedo, F. A.; de Pablo, J. J. On the Simulation of Vapor−Liquid Equilibria for Alkanes. *J. Chem. Phys.* **1998**, *108*, 9905.

(9) Ungerer, P.; Tavitian, B.; Boutin, A. *Applications of Molecular Simulation in the Oil and Gas Industry*; Editions Technip: Paris, 2006.

(10) Sonnet, A. M.; Maffettone, P. L.; Virga, E. G. Continuum Theory for Nematic Liquid Crystals with Tensorial Order. *J. Non-Newtonian Fluid Mech.* **2004**, *119*, 51.

(11) Qian, T.; Sheng, P. Generalized Hydrodynamic Equations for Nematic Liquid Crysyals. *Phys. Rev. E* **1998**, *58*, 7475.

(12) Müller-Plathe, F. Coarse-Graining in Polymer Simulation: From the Atomistic to Mesoscopic Scale and Back. *Chem. Phys. Chem.* **2002**, *3*, 754.

(13) Reith, D.; Pütz, M.; Müller-Plathe, F. Deriving Effective Mesosclale Potentials from Atomistic Simulations. *J. Comput. Chem.* **2003**, *24*, 1624.

(14) Sun, Q.; Faller, R. Systematic Coarse-Graining of Atomistic Models for Simulation of Polymeric Systems. *Comput. Chem. Eng.* **2005**, *29*, 2380.

(15) Milano, G.; Müller-Plathe, F. Mapping Atomistic Simulations to Mesoscopic Models: A Systematic Coarse-Graining Procedure for Vinyl Polymer Chains. *J. Phys. Chem. B* **2005**, *109*, 18609.

(16) Vettorel, T.; Meyer, H. Coarse-Graining of Short Polythylene Chains for Studying Polymer Crystallization. *J. Chem. Theory Comput.* **2006**, *2*, 616.

(17) Jain, S.; Garde, S.; Kumar, S. K. Do Inverse Monte Carlo Algorithms Yield Thermodynamically Consistent Interaction Potentials. *Ind. Eng. Chem. Res.* **2006**, *45*, 5614.

(18) Spyriouni, T.; Tzoumanekas, C.; Theodorou, D. N.; Müller-Plathe, F.; Milano, G. Coarse-Grained and Reverse-Mapped United-Atom Simulations of Long-Chain Atactic Polysterene Melts: Structure, Thermodynamic Properties, Chain Conformation, and Entanglements. *Macromolecules* **2007**, *40*, 3876.

(19) Kamio, K.; Moorthi, K.; Theodorou, D. N. Coarse-Grained End Bridging Monte Carlo Simulations of Poly(ethyleneterephthalate) Melt. *Macromolecules* **2007**, *40*, 710–722.

(20) Faller, R.; Schmitz, H.; Biermann, O.; Müller-Plathe, F. Automatic Parameterization of Force Fields for Liquids by Simplex Optimization. *J. Comput. Chem.* **1999**, *20*, 1009.

(21) Meyer, H.; Biermann, O.; Faller, R.; Reith, D.; Müller-Plathe, F. Coarse Graining of Nonbonded Inter-Particle Potentials Using Automatic Simplex Optimization to Fit Structural Properties. *J. Chem. Phys.* **2000**, *113*, 6264.

(22) Reith, D.; Meyer, H.; Müller-Plathe, F. Mapping Atomistic to Coarse-Grained Polymer Models Using Automatic Simplex Optimization to Fit Structural Properties. *Macromolecules* **2001**, *34*, 2335.

(23) Faller, R. Automatic Coarse Graining of Polymers. *Polymer* **2004**, *45*, 3869.

(24) Marrink, S. J.; de Vries, A. H.; Mark, A. E. Coarse Grained Model for Semiquantitative Lipid Simulations. *J. Phys. Chem. B* **2004**, *108*, 750.

(25) Shelley, J. C.; Shelley, M. Y.; Reeder, R. C.; Bandyopadhyay, S.; Klein, M. L. A Coarse Grain Model for Phospholipid Simulations. *J. Phys. Chem. B* **2001**, *105*, 4464.

(26) Stevens, M. J.; Hoh, J. H.; Woolf, T. B. Insights into the Molecular Mechanism of Membrane Fusion from Simulation: Evidence for the Association of Splayed Tails. *Phys. Rev. Lett.* **2003**, *91*, 188102.

(27) Tozzini, V. Coarse-Grained Models for Proteins. *Curr. Opin. Struct. Biol.* **2005**, *15*, 144.

(28) Izvekov, S.; Voth, G. A. A Multiscale Coarse-Graining Method for Biomolecular Systems. *J. Phys. Chem. B* **2005**, *109*, 2469.

(29) Izvekov, S.; Voth, G. A. Multiscale Coarse Graining of Liquid-State Systems. *J. Chem. Phys.* **2005**, *123*, 134105.

(30) Noid, W. G.; Chu, J.; Ayton, G. S.; Voth, G. A. Multiscale Coarse-Graining and Structural Correlations: Connections to Liquid-State Theory. *J. Phys. Chem. B* **2007**, *111*, 4116.

(31) Voth, G. A. *Coarse-Graining of Condensed Phase and Biomolecular Systems*; CRC Press: Boca Raton, FL, 2008.

(32) Lyubartsev, A. P.; Laaksonen, A. Calculation of Effective Interaction Potentials from Radial Distribution Functions: A Reverse Monte Carlo Approach. *Phys. Rev. E* **1995**, *52*, 3730.

(33) Brake, J. M.; Daschner, M. K.; Luk, Y.; Abbott, N. L. Biomolecular Interactions at Phospholipid-Decorated Surfaces of Liquid Crystals. *Science* **2003**, *302*, 2094.

(34) Lockwood, N. A.; Abbott, N. L. Self-Assembly of Surfactants and Phospholipids at Interfaces between Aqueous Phases and Thermotropic Liquid Crystals. *Curr. Opin. Colloid Interface Sci.* **2005**, *10*, 111.

(35) Brake, J. M.; Daschner, M. K.; Abbott, N. L. Formation and Characterization of Phospholipid Monolayers Spontaneously Assembled at Interfaces between Aqueous Phases and Thermotropic Liquid Crystals. *Langmuir* **2005**, *21*, 2218.

(36) Chandrasekhar, S. *Liquid Crystals*, revised ed.; Cambridge University Press: Cambridge, U.K., 1990.

(37) Denk-Ke, Y.; Shin-Tson, W. *Fundamentals of Liquid Crystal Devices*; Wiley Series in Display Technology; Wiley: West Sussex, U.K., 2006.

(38) Gay, J. G.; Berne, B. Modification of the Overlap Potential to Mimic a Linear Site-Site Potential. *J. Chem. Phys.* **1981**, *74*, 3316.

(39) Frenkel, D. Computer Simulation of Hard-Core Models for Liquid Crystals. *Mol. Phys.* **1987**, *60*, 1.

(40) Allen, M. P.; Frenkel, D.; Talbot, J. Molecular Dynamics Simulation Using Hard Particles. *Comput. Phys. Rep.* **1989**, *9*, 301.

(41) Whittle, M.; Masters, A. J. Liquid Crystal Formation in a System of Fused Hard Spheres. *Mol. Phys.* **1991**, *72*, 247.

(42) Allen, M. P.; Evans, G. T.; Frenkel, D.; Mulder, B. M. Hard Convex Body Fluids. *Adv. Chem. Phys.* **1993**, *86*, 1.

(43) Williamson, D. C.; Jackson, G. Liquid Crystalline Phase Behavior in Systems of Hard-Sphere Chains. *J. Chem. Phys.* **1998**, *108*, 10294.

(44) Wilson, M. R. Molecular Modelling of Liquid Crystal Systems: An Internal Coordinate Monte Carlo Approach. *Liq. Cryst.* **1996**, *21*, 437.

(45) Lansac, Y.; Glaser, M. A.; Clark, N. A. Microscopic Structure and Dynamics of a Partial Bilayer Smectic Liquid Crystal. *Phys. Rev. E* **2001**, *64*, 051703.

(46) Zakharov, A. V.; Maliniak, A. Structure and Elastic Properties of a Nematic Liquid Crystal: A Theoretical Treatment and Molecular Dynamics Simulation. *Eur. Phys. J. E* **2001**, *4*, 85.

(47) Zakharov, A. V.; Maliniak, A. Theoretical Investigations of Rotational Phenomena and Dielectric Properties in a Nematic Liquid Crystal. *Eur. Phys. J. E* **2001**, *4*, 435.

(48) Cheung, D. L.; Clark, S. J.; Wilson, M. R. Parameterization and Validation of a Force Field for Liquid-Crystal Forming Molecules. *Phys. Rev. E* **2002**, *65*, 051709.

(49) Cacelli, I.; Prampollini, G.; Tani, A. Atomistic Simulation of a Nematogen Using a Force Field Derived from Quantum Chemical Calculations. *J. Phys. Chem. B* **2005**, *109*, 3531.

(50) De Gaetani, L.; Prampollini, G.; Tani, A. Modeling a Liquid Crystal Dynamics by Atomistic Simulation with Ab Initio Derived Force Field. *J. Phys. Chem. B* **2005**, *110*, 2847.

(51) Tiberio, G.; Muccioli, L.; Berardi, R.; Zannoni, C. Towards *in Silico* Liquid Crystals. Realistic Transition Temperatures and Physical Properties for *n*-Cyano-Biphenyls via Molecular Dynamics Simulations. *ChemPhysChem* **2008**, *9*, 1.

(52) Peter, C.; Delle Site, L.; Kremer, K. Classical Simulations from the Atomistic to the Mesoscale and back: Coarse Graining an Azobenzene Liquid Crystal. *Soft Matter* **2008**, *4*, 859.

(53) Luckhurst G.; Gray, G. W. *The Molecular Physics of Liquid Crystals*; Academic Press: London, 1979.

(54) Hird, M. Nematics. *Physical Properties of Liquid Crystals*; IEE: London, 2001; Vo1. *1*, pp 3−16.

(55) de Gennes, P. G. *The Physics of Liquid Crystals*; Clarendon Press: Oxford, U.K., 1974.

(56) Wilson, M. R.; Allen, M. P. Structure of Trans-4-(*trans*-4-*n*-pentylcyclohexyl)cyclohexylcarbonitrile (CCHS) in the Isotropic and Nematic Phases: A Computer Simulation Study. *Liq. Cryst.* **1992**, *12*, 157.

(57) Eppenga, R.; Frenkel, D. Monte Carlo Study of the Isotropic and Nematic Phases of Infinitely Thin Hard Platelets. *Mol. Phys.* **1984**, *52*, 1303.

(58) Luckhurst, G. R.; Veracini, C. A. *The Molecular Dynamics of Liquid Crystal*; NATO ASI Series; Kluwer Academic Publishers: Dordrecht, The Netherlands, 1994.

(59) Henderson, R. L. A Uniqueness Theorem for Fluid Pair Correlation Functions. *Phys. Lett. A* **1974**, *49*, 197.

(60) Lyubartsev, A. P.; Laaksonen, A. Osmotic and Activity Coefficients from Effective Potentials for Hydrated Ions. *Phys. Rev. E* **1997**, *55*, 5689.

(61) Soper, A. K. Empirical Potential Monte Carlo Simulation of Fluid Structure. *Chem. Phys.* **1996**, *202*, 295.

(62) Gϕo, N.; Scheraga, H. A. On the Use of Classical Statistical Mechanics in the Treatment of Polymer Chain Conformation. *Macromolecules* **1976**, *9*, 535.

(63) Berendsen, H. J. C.; van der Spoel, D.; van Drunen, R. GROMACS: A Message-Passing Parallel Molecular Dynamics Implementation. *Comput. Phys. Commun.* **1995**, *91*, 43.

(64) Van der Spoel, D.; Lindahl, E.; Hess, B.; Groenhof, G.; Mark, A. E.; Berendsen, H. J. C. GROMACS: Fast, Flexible and Free. *J. Comput. Chem.* **2005**, *26*, 1701.

(65) van der Spoel, D.; Lindahl, E.; Hess, B.; van Buuren, A. R.; Apol, E.; Meulenhoff, P. J.; Sijbers, A.; Feenstra, K. A.; van Drumen, R.; Berendsen, H. J. C. *GROMACS User Manual*, version 3.3; University of Groningen: Groningen, The Netherlands, 2005.

(66) Ryckaert, J. P.; Ciccotti, G.; Berendsen, H. J. C. Numerical Integration of the Cartesian Equations of Motion of a System with Constraints: Molecular Dynamics of *n*-Alkanes. *J. Comput. Phys.* **1977**, *23*, 327.

(67) Nose, S. A Molecular Dynamics Method for Simulations in the Canonical Ensemble. *Mol. Phys.* **1984**, *52*, 255.

(68) Hoover, W. G. Canonical Dynamics: Equilibrium Phase-Space Distributions. *Phys. Rev. A* **1985**, *31*, 1695.

(69) Parrinello, M.; Rahman, A. Polymorphic Transitions in Single Crystals: A New Molecular Dynamics Method. *J. Appl. Phys.* **1981**, *52*, 7182.

(70) Nosé, S.; Klein, M. L. Constant Pressure Molecular Dynamics for Molecular Systems. *Mol. Phys.* **1983**, *50*, 1055.

(71) Galassi, M.; Davies, J.; Theiler, J.; Gough, B.; Jungman, G.; Booth, M.; Rossi, F. *GNU Scientific Library Reference Manual* 2nd ed.; Network Theory Ltd.: Bristol, 2006.

(72) Broucke, R. Algorithm: Ten Subroutines for the Manipulation of Chebyshev Series. *Commun. ACM* **1973**, *16*, 254.

(73) Wuerflinger, A.; Sandmann, H. Nematics. *Physical Properties of Liquid Crystals*; IEE: London, 2001; Vol. 1.

(74) Allen, M. P.; Tildesley, D. J. *Computer Simulation of Liquids*; Clarendon Press:Oxford, U.K., 1987.

(75) Van Kampen, N. G. *Stochastic Processes in Physics and Chemistry*; North-Holland: Amsterdam, The Netherlands, 1981).

(76) Zwanzig, R. Memory Effects in Irreversible Thermodynamics. *Phys. Rev.* **1961**, *124*, 983.

(77) Mori, H. A Continued-Fraction Representation of the Time-Correlation Functions. *Prog. Theor. Phys.* **1965**, *34*, 399.

(78) Hijon, C.; Espanol, P.; Vanden-Eijnden, E.; Delgado-Buscalioni, R. Mori−Zwanzig Formalism as a Practical Tool. *Faraday Discuss.* **2010**, *144*, 301.

(79) Kruger, G. J. Diffusion in Thermotropic Liquid Crystals. *Phys. Rep.* **1982**, *82*, 229.

(80) De Gaetani, L.; Prampolini, G. Computational Study through Atomistic Potentials of a Partial Bilayer Liquid Crystal: Structure and Dynamics. *Soft Matter* **2009**, *5*, 3517.

(81) Sandmann, H.; Hamann, F.; Wurflinger, A. PVT Measurements on 4-*n*-Pentyl-4′-Cyano-Biphenyl (5CB) and *trans*-4-(4′-Octyl-Cyclohexyl)-Benzonitrile (8PCH) up to 300 MPa. *Z. Naturforsch. A* **1997**, *52*, 739.

(82) Horn, R. G. Refractive Indices and Order Parameters of Two Liquid Crystals. *J. Phys. Paris* **1978**, *39*, 105.